

## Aromatic inorganic acid radical

Jiawen Zhou<sup>1†</sup>, Weiya Zhu<sup>1†</sup>, Miao Zeng<sup>1</sup>, Qingqing Yang<sup>2</sup>, Ping Li<sup>2</sup>, Linfeng Lan<sup>1</sup>,  
Junbiao Peng<sup>1</sup>, Yuan Li<sup>1\*</sup>, Fei Huang<sup>1\*</sup> & Yong Cao<sup>1</sup>

<sup>1</sup>State Key Laboratory of Luminescent Materials and Devices, Institute of Polymer Optoelectronic Materials and Devices, South China University of Technology, Guangzhou 510640, China;

<sup>2</sup>Key Laboratory for Organic Electronics and Information Displays & Institute of Advanced Materials, Jiangsu National Synergetic Innovation Center for Advanced Materials, Nanjing University of Posts & Telecommunications, Nanjing 210023, China

Received August 19, 2019; accepted October 14, 2019; published online November 26, 2019

Stable radicals are challenging to prepare due to their intrinsic high reactivity. Herein, three trisphenolamine radicals were readily synthesized and exhibited unexpected thermal/electrochemical stability and semiconductor property. These three nitroxide radicals could be considered as a class of aromatized nitro groups or HNO<sub>3</sub> derivatives. The closed-shell nitro-like and open-shell nitroxide resonance structure contribute to their outstanding stability. Furthermore, the tunable ground states, extremely low band gap and p-type charge transport properties were systematically investigated. More importantly, the work presents the concept of aromatic inorganic acid radical (AIAR) and aggregation-induced radical (AIR) mechanism to understand the intrinsic structure-property relationship of these radicals. In addition, we provide a novel strategy for the design of stable and low bandgap radicals for organic electronics, magnetics, spintronics, etc.

**organic electronics, aromatic nitric acid radical, aggregation-induced radical, polycyclic aromatic hydrocarbons, spintronics**

**Citation:** Zhou J, Zhu W, Zeng M, Yang Q, Li P, Lan L, Peng J, Li Y, Huang F, Cao Y. Aromatic inorganic acid radical. *Sci China Chem*, 2019, 62, <https://doi.org/10.1007/s11426-019-9641-2>

### 1 Introduction

Organic radical molecules have recently aroused a growing interest due to their unique electronic [1], nonlinear optical [2] and magnetic properties [3], and promising applications in luminescent materials [4], organic spintronics [5], thermoelectric materials [6], and energy storage devices [7]. However, these materials often exhibit molecular instability due to their intrinsic high reactivity, which will limit their practical applications [8]. Since the Thiele's and Chichibabin's hydrocarbon were reported [9,10], much efforts have been devoted to exploring stable organic radicals [11–13]. Numerous localized diradicals and delocalized diradicals were successfully prepared based on creative designs to

lower the reactivity of radical species and enhance stability [14–16]. The localized radical molecules can greatly reduce the possibility of reactions in chemical kinetics and thus exhibit good stability due to steric hindrance effect [17]. Polycyclic aromatic hydrocarbons (PAHs) with singlet ground states are relatively stable to oxygen, light or heat due to kinetic blocking [18–20]. The stable zethrenes can even be stored in the air for a month [21]. Moreover, the typical nitroxide radical group 2,2,6,6-tetramethylpiperidin-1-oxyl (TEMPO) exhibits excellent air-stability and achieves extensive applications under the protection of four methyl groups [22–24]. The extension of the  $\pi$  conjugation is another promising strategy for isolating unstable radical molecules [25,26]. The Kekule-type delocalized diradicals could be less reactive to molecular oxygen due to the use of a smaller aromatic stabilization energy and thermodynamic stabilization of the radical moiety [27,28].

<sup>†</sup>These authors contributed equally to this work.

\*Corresponding authors (email: [celiy@scut.edu.cn](mailto:celiy@scut.edu.cn); [msfhuang@scut.edu.cn](mailto:msfhuang@scut.edu.cn))

In the previous work, TEMPO radicals show high stability due to the steric hindrance and reversible redox property based on their electron transfer process between open-shell TEMPO radical and TEMPOonium (Scheme 1(a)) [29]. Phenoxy radical shows relative stability due to the radical delocalization on the quinoid structure. In order to enhance the stability of phenoxy radical, the galvinoxyl radicals with *tert*-butyl groups were successfully prepared and exhibited excellent steric stability, along with the emergence of quinoid structure and spin delocalization of unpaired electron over the whole of the conjugated skeleton [30,31]. Another galvinoxyl derivative Yang's biradical (Scheme 1 (b)) with three phenoxy radicals exhibited biradical property because of the formation of covalent bond between the unpaired p electron of the methine carbon atom and any radical spin [32]. Sakamaki *et al.* [33] prepared a novel triphenylamine derivative having two phenoxy radicals by substituting nitrogen atom for central carbon atom (Scheme 1(b)). The triphenylamine phenoxy radical showed the unexpected stability due to the closed-shell electronic structure and two unusual C–N bonds with multiple-bond character.

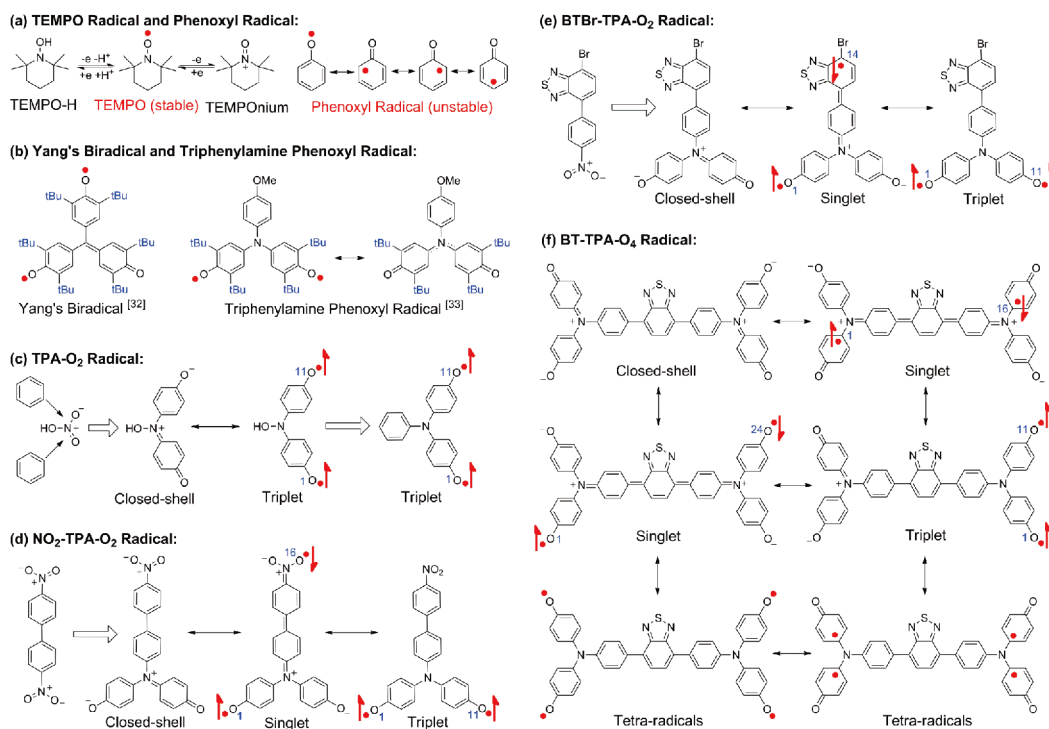
In order to further stabilize the triphenylamine phenoxy radicals, we proposed to introduce the conjugated nitroxides without any steric protection to prepare the semiconductive radicals with good stability by delocalizing unpaired electrons and introducing electron-withdrawing groups (Scheme 1). These neutral conjugated nitroxides NO<sub>2</sub>-TPA-O<sub>2</sub>, BTBr-

TPA-O<sub>2</sub> and BT-TPA-O<sub>4</sub> were successfully synthesized and exhibited excellent thermal/electrochemical stability, compared to the traditional water-oxygen sensitive radical cations of triarylamines [34–36]. The proposed closed-shell quinoid structure of conjugated nitroxides is stable, and is accompanied by a variety of resonance structures containing unpaired electrons, as indicated in Scheme 1. Moreover, we discovered that the closed-shell resonance structure is marvelously similar to the structure of nitro group, which explains the stability of these radical molecules. Considering the large challenge to obtain air-stable radicals with triplet ground states [37], the TPA-O<sub>2</sub>, NO<sub>2</sub>-TPA-O<sub>2</sub> and BTBr-TPA-O<sub>2</sub> might exhibit triplet ground states due to the odd number (1-/11-) positions of their two radicals in these molecules, respectively. Interestingly, we found NO<sub>2</sub>-TPA-O<sub>2</sub> and BTBr-TPA-O<sub>2</sub> also exhibited singlet ground states with the resonance structures in which the diradicals were distributed on even positions. The novel mechanism of aromatic inorganic acid radicals (AIAR) was proposed to understand their chemical/physical properties in the following discussion.

## 2 Experimental

### 2.1 Materials

All the materials were purchased from commercial sources



**Scheme 1** Resonance structures of radical motivated from aromatic HNO<sub>3</sub>. (a) The redox behavior of Tempo radical and unstable phenoxy radical; (b) structures of Yang's biradical [32] and triphenylamine phenoxy radical [33]; the resonance structures of (c) TPA-O<sub>2</sub> radical, (d) NO<sub>2</sub>-TPA-O<sub>2</sub> radical, (e) BTBr-TPA-O<sub>2</sub> radical and (f) BT-TPA-O<sub>4</sub> radical motivated from aromatic HNO<sub>3</sub>. The resonance structures of singlet and triplet states are driven by the AIR mechanism and the thermal excitation, respectively (color online).

and used as received. The raw materials used in the experiment were as follows: 4-methoxy-*N*-(4-methoxyphenyl)-*N*-(4-(4,4,5,5-tetramethyl-1,3,2-dioxaborolan-2-yl)phenyl)aniline, 4,7-dibromobenzo[*c*][1,2,5] thiadiazole, 4-bromo-1-nitrobenzene and 4,4'-dimethoxytriphenylamine. The detailed synthesis of compounds NO<sub>2</sub>-TPA-O<sub>2</sub>, BTBr-TPA-O<sub>2</sub> and BT-TPA-O<sub>4</sub> were presented in Scheme 2.

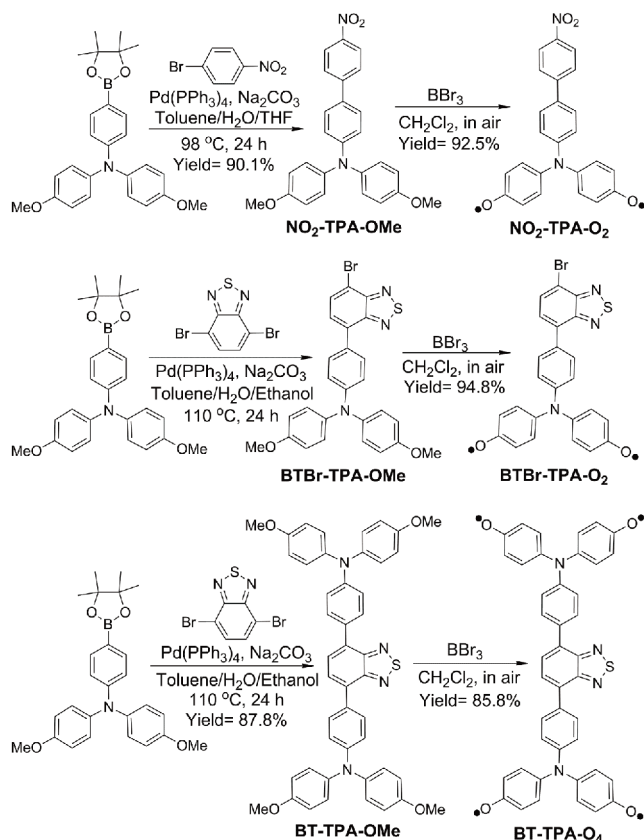
## 2.2 Measurements

The <sup>1</sup>H NMR spectra of samples were recorded by DRX-400 or 600 spectrometer (400 and 500 MHz <sup>1</sup>H NMR frequency, Bruker Co., Germany) in CDCl<sub>3</sub> or DMSO-*d*<sub>6</sub> at room temperature. The ultraviolet visible near-infrared (UV-Vis-NIR) spectra were obtained by a UV-3600 spectrophotometer (SHIMADZU Co., Japan). Cyclic voltammetry (CV) was performed in CH<sub>2</sub>Cl<sub>2</sub> solution with 0.1 M tetrabutylammonium hexafluorophosphate (Bu<sub>4</sub>NPF<sub>6</sub>) as the supporting electrolyte at a scan rate of 100 mV/s, a Hg/HgCl<sub>2</sub> (Saturated KCl solution) electrode as the reference electrode, a carbon-glass electrode as the working electrode, a Pt line electrode as the counter electrode and ferrocene/ferrocenium (Fc/Fc<sup>+</sup>) as an internal reference on electrochemistry workstation (CHI660E, China). Electron spin resonance (ESR) spectra were measured on a Bruker ELEXSYS-II E500 CW-EPR

spectrometer (Germany). ESR spectra of samples were recorded at a signal attenuation of 16 dB. Dewars used to support thermocouples were different for low temperature and high temperature tests. Quartz EPR standard quality tubes with an outer diameter of 3 mm were purchased from Beijing Synthware Glass Inc. (China). A Quantum Design 7 Tesla SQUID-VSM system was available for the magnetic measurement in this work. Powder sample was sealed in a plastic capsule. Magnetic moment was measured in the temperature range of 2 to 400 K, with an applied field of 500 Oe. The empty plastic capsule exhibited diamagnetic and its magnetic moment was measured for correction. The modified Bleaney-Bowers equation that was used for the curve fitting as follow:

$$\chi = \frac{Ng^2\mu_B^2}{kT} \left[ \frac{2}{3 + e^{-2J/kT}} \right] (1 - \rho) + \frac{Ng^2\mu_B^2}{2kT} \rho + \text{TIP}(1 - \rho)$$

where  $\rho$  is the fraction of  $s=1/2$  impurity, TIP is the temperature independent paramagnetism due to a small energy gap between ground singlet state and excited triplet state. Density functional theory (DFT) calculations were performed with the Gaussian 09 suite of programs. The geometry optimizations of methoxy and hydroxyl substituted precursors were carried out at B3LYP/6-31G\* level of theory and the optimized geometries of radical counterparts were performed with UB3LYP/6-31G\* level of theory on the singlet ground state [38,39]. The single energy and spin density distribution of three kinds of neutral conjugated nitroxide radicals in the closed-shell, open-shell singlet and open-shell triplet states were performed with B3LYP/6-311++G\*\* level of theory.



**Scheme 2** Synthetic routes for NO<sub>2</sub>-TPA-O<sub>2</sub>, BTBr-TPA-O<sub>2</sub> and BT-TPA-O<sub>4</sub>.

## 2.3 The fabrication of the hole-only devices

The hole-only devices were fabricated with the structure of indium tin oxides (ITO)/HTM/Ag and ITO/PEDOT:PSS/HTM/MoO<sub>3</sub>/Ag. BT-TPA-OMe or BT-TPA-O<sub>4</sub> solutions were prepared in toluene or ethanol (20 mg/mL), respectively, stirred at 50 °C for 10 h and filtered it with a 0.22 μm filter element. The ITO-coated glass substrates were cleaned by sonication in detergent, deionized water, acetone, and isopropyl alcohol and dried in an oven at 75 °C for 10 h. PEDOT:PSS aqueous solution was spin-coated at 3,500 r/min for 30 s (thickness of 30 nm) and thermally annealed at 145 °C on a hotplate for 15 min in the air. The layer of BT-TPA-OMe or BT-TPA-O<sub>4</sub> was spin-coated on PEDOT:PSS film at 800–2,000 r/min. A 10 nm MoO<sub>3</sub> layer and a 100 nm Ag layer were subsequently evaporated through a shadow mask to define the active area of the devices (0.0516 cm<sup>2</sup>) and form a top anode. All of the fabrication processes were performed inside a controlled atmosphere of nitrogen glove box (Vacuum Atmosphere, USA) that contained less than

10 ppm oxygen and moisture. The current density-voltage ( $J$ - $V$ ) characteristics of hole-only devices were measured with a Keithley 236 sourcemeter under dark. The experimental  $J$ - $V$  characteristics of hole-only devices are given by

$$J_{\text{SCLC}} = \frac{9}{8} \varepsilon_0 \varepsilon_r \mu_p \frac{V^2}{d^3}$$

where  $\varepsilon_0$ ,  $\varepsilon_r$ ,  $\mu_p$  and  $d$  are the permittivity, hole mobility at low voltage and thickness of the hole transport layer, respectively. Using a relative dielectric constant  $\varepsilon_r$  of 3 and built-in voltage  $V_{\text{bi}}=1.5$  V, it is observed from the slope of the  $\log(J)$  versus  $\log(V)$  plot [40] that the current density depends quadratically on the voltage. The applied voltage should be corrected for the voltage drop across the ITO series resistance  $V_{\text{Rs}}$ , which amounts to 10  $\Omega$  in these substrates [41].

## 2.4 General procedures for the preparation of NO<sub>2</sub>-TPA-OMe, BTBr-TPA-OMe and BT-TPA-OMe

4,4'-(2,1,3-Benzothiadiazole-4,7-diyl)bis[*N,N*-bis(4-methoxyphenyl)benzenamine (BT-TPA-OMe), *N,N*-bis(4-methoxyphenyl)-4'-nitro[1,1'-biphenyl]-4-amine (NO<sub>2</sub>-TPA-OMe) were simply prepared by Suzuki coupling in 87.8% and 90.1% yield, respectively, which were the tetrakis(triphenylphosphine) palladium Pd(PPh<sub>3</sub>)<sub>4</sub> (0.05 eq.)-catalyzed cross coupling between 4-methoxy-*N*-(4-methoxyphenyl)-*N*-(4-(4,4,5,5-tetramethyl-1,3,2-dioxaborolan-2-yl)phenyl)aniline (2.5 eq.) and 4,7-dibromobenzo[*c*][1,2,5]thiadiazole (1 eq.) as well as 4-methoxy-*N*-(4-methoxyphenyl)-*N*-(4-(4,4,5,5-tetramethyl-1,3,2-dioxaborolan-2-yl)phenyl)aniline (1 eq.) and 4-bromo-1-nitrobenzene (1 eq.). These raw materials were dissolved in a mixture of degassed toluene (15 mL), ethanol (5 mL) or tetrahydrofuran (THF, 10 mL) and Na<sub>2</sub>CO<sub>3</sub> (2 M, 2 mL) in a 100 mL two-necked round bottomed flask under nitrogen atmosphere. The mixture was refluxed for 24 h under nitrogen atmosphere. Next, the solvent was removed under vacuum and the organic phase was extracted three times with water and dichloromethane. After concentration, the crude compound was purified by silica gel column chromatography (eluted:dichloromethane/petroleum ether=1:2, *v/v*) to give BT-TPA-OMe and NO<sub>2</sub>-TPA-OMe. Besides, 4-(7-bromo-2,1,3-benzothiadiazol-4-yl)-*N,N*-bis(4-methoxyphenyl)benzenamine (BTBr-TPA-OMe) was obtained from by-product recovery during the preparation of BT-TPA-OMe. The final powder product was sent to vacuum drying at 55 °C for 24 h.

## 2.5 General procedures for the preparation of NO<sub>2</sub>-TPA-O<sub>2</sub>, BTBr-TPA-O<sub>2</sub> and BT-TPA-O<sub>4</sub>

Synthesis of 4,4',4'',4'''-[2,1,3-benzothiadiazole-4,7-diyl]bis(4,1-phenylenenitrilo)] tetrakis-phenol (BT-TPA-O<sub>4</sub>), *N,N*-bis(4-hydroxyphenyl)-4'-nitro[1,1'-biphenyl]-4-amine

(NO<sub>2</sub>-TPA-O<sub>2</sub>) and 4-(7-bromo-2,1,3-benzothiadiazol-4-yl)-*N,N*-bis(4-hydroxyphenyl) benzenamine (BTBr-TPA-O<sub>2</sub>) was shown in Scheme 2: BT-TPA-OMe (1 eq.), NO<sub>2</sub>-TPA-OMe (1 eq.) or BTBr-TPA-OMe (1 eq.) in dry CH<sub>2</sub>Cl<sub>2</sub> (15 mL) was cooled to -70 °C by ethanol in cold trap, and then BBr<sub>3</sub> (10 eq. or 5 eq.) was added dropwise under N<sub>2</sub> over 5 min. The mixture was then stirred at room temperature for 12 h under nitrogen atmosphere with precipitation of solid product. Methanol (15 mL) was added dropwise into the reacting solution to quench BBr<sub>3</sub>. After dropping the solution into deionized water, the solids can be separated by filtration and the crude product was purified by washing with H<sub>2</sub>O and CH<sub>2</sub>Cl<sub>2</sub> successively. The crude compounds were purified by silica gel column chromatography (eluted:ethanol/petroleum ether=3:1, *v/v*) to obtain target products. The final powder products were sent to vacuum drying at 60 °C for 24 h. The oxidation products BT-TPA-O<sub>4</sub>, NO<sub>2</sub>-TPA-O<sub>2</sub> and BTBr-TPA-O<sub>2</sub> could be obtained by exposing powder to air.

## 3 Results and discussion

### 3.1 The design of aromatic nitric acid radicals

Initially viewing the chemical structure of HNO<sub>3</sub>, we proposed to insert two phenyl groups into HNO<sub>3</sub> and thus obtained the stable diradical TPA-O<sub>2</sub> with triplet ground state as the aromatic group produced the electron delocalization effect of free electrons of TPA-O<sub>2</sub> (Scheme 1(c)). TPA-O<sub>2</sub> would process two resonance structures including closed-shell nitro-like and open-shell diradical. We prepared TPA-OH<sub>2</sub> and tried to obtain TPA-O<sub>2</sub> diradical by oxidation of TPA-OH<sub>2</sub>. Finally, we found the TPA-O<sub>2</sub> was not stable and the single crystal of TPA-OH<sub>2</sub> was collected as presented in Figure 1 [42]. It can be observed that the hydrogen bond length of TPA-OH<sub>2</sub> is 1.935 Å, illustrating hydrogenation of unstable triplet ground state. Besides, strong electron-withdrawing groups such as nitro and benzothiadiazole (BT) were introduced to further stabilize unpaired electrons. Both NO<sub>2</sub>-TPA-O<sub>2</sub> (Scheme 1(d)) and BTBr-TPA-O<sub>2</sub> (Scheme 1(e)) will process several resonance structures including the nitro-like closed-shell structure, as well as open-shell structures with potential singlet and triplet states due to the co-existence of even/odd positions of diradicals. This is distinct from canonical resonance structures (Scheme 1(b)) proposed in previous work [33]. This interesting and reasonable hypothesis makes us successfully achieve the tunable ground states of this type of diradicals, which is of great importance for this field [21]. In order to further enhance the radical delocalization, the symmetrical bisphenolamine radicals are introduced to increase the conjugation length and BT-TPA-O<sub>4</sub> is designed and expected to show stable diradical property due to its more diverse structural resonances comparing with previous ones.

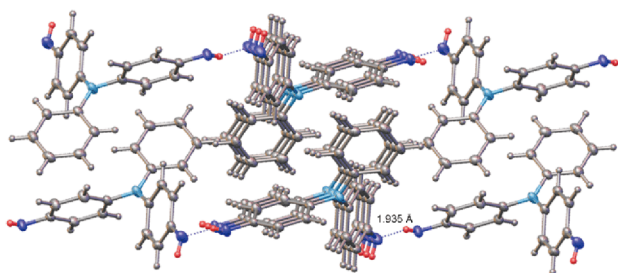


**Figure 1** X-ray crystallographic structure and crystal packing of TPA-OH<sub>2</sub> at 100 K (color online).

NO<sub>2</sub>-TPA-O<sub>2</sub> and BTBr-TPA-O<sub>2</sub> were successfully synthesized to investigate the effect of conjugation and electron-withdrawing effect on formation of nitroxide radicals. NO<sub>2</sub>-TPA-O<sub>2</sub> exhibits unique performance that the disappearance of <sup>1</sup>H NMR spectrum signal (Figure S4, [Supporting Information online](#)) and the absorption at 600–800 nm in UV-Vis-NIR absorbance spectrum in solution (Figure 2(a)). These results clearly demonstrate the existence of radicals for NO<sub>2</sub>-TPA-O<sub>2</sub> in solution. The absorption characteristics of BTBr-TPA-OH<sub>2</sub> are consistent with that of BTBr-TPA-OMe in solution, indicating the dominant hydroxyl groups rather than phenoxy radical. The highly conjugated backbone boosts to new visible or NIR absorption of NO<sub>2</sub>-TPA-O<sub>2</sub> and BTBr-TPA-O<sub>2</sub> at 527 nm in Figure 2(a) and 660 nm in Figure 2(b) in film, respectively. The black powder of NO<sub>2</sub>-TPA-O<sub>2</sub> or BTBr-TPA-O<sub>2</sub> is also in good agreement with the absorption of radicals in the visible region.

The typical peaks of UV-Vis absorption appeared at 480 and 485 nm for BT-TPA-OMe and BT-TPA-OH<sub>4</sub> in solution, respectively. It was in good agreement with expected behavior that demethylation had ultra-weak effect on absorption in the visible region [43]. However, the situation is quite different in film, as depicted in Figure 2(c). BT-TPA-O<sub>4</sub> showed a typical absorption peak in the range of 450–1,000 nm, which showed great red shift comparing with that of BT-TPA-OMe. It can be explained that the transformation of OH groups of BT-TPA-OH<sub>4</sub> to phenoxy radicals is occurring and the resonance structural characteristics of tetra-radicals are dominated after being exposed to air. Besides, we noticed that the color of BT-TPA-O<sub>4</sub> in powder was black but dilute solution was dull red, compared to the red BT-TPA-OMe in both solid and solution state. It is recognized that the intrinsic BT-TPA-OH<sub>4</sub> is red like BT-TPA-OMe if the OH groups are still in the backbone of BT-TPA-OH<sub>4</sub> but BT-TPA-O<sub>4</sub> is black due to radical formation [43]. Accordingly, a small amount of BT-TPA-OH<sub>4</sub> is easily oxidized in air and regenerated under interaction with proton in water. The distinct absorption and black powders of NO<sub>2</sub>-TPA-O<sub>2</sub>, BTBr-TPA-O<sub>2</sub> and BT-TPA-O<sub>4</sub> in film demonstrate the existence of radicals. In addition, we did not detect the

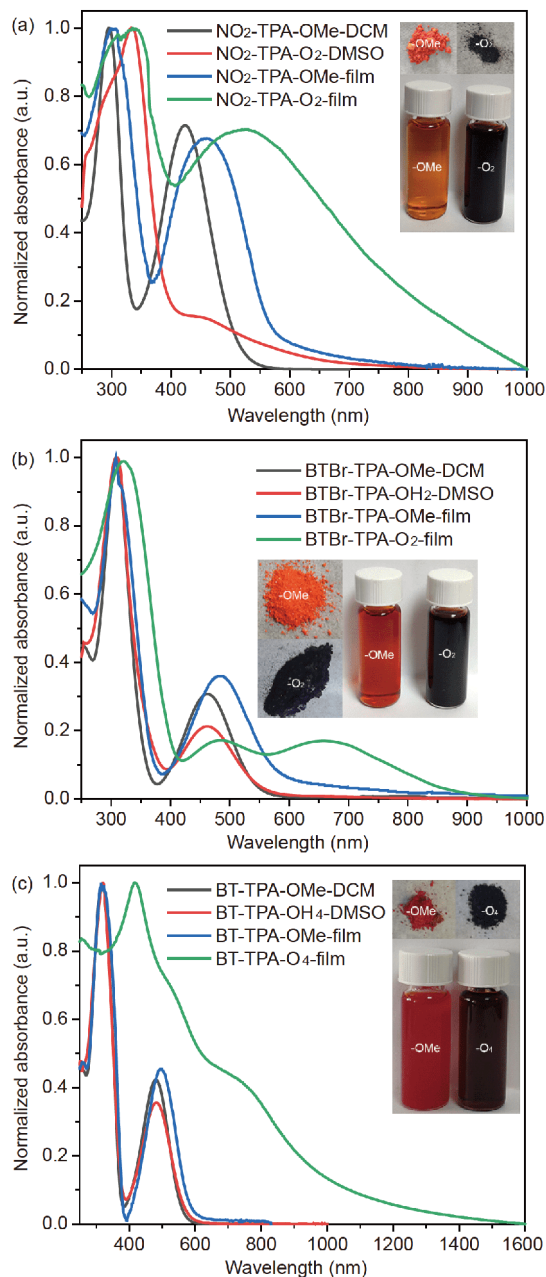


**Figure 2** UV-Vis-NIR spectra of (a) NO<sub>2</sub>-TPA-OMe and NO<sub>2</sub>-TPA-O<sub>2</sub>, (b) BTBr-TPA-OMe and BTBr-TPA-O<sub>2</sub>, (c) BT-TPA-OMe and BT-TPA-O<sub>4</sub> in solution as well as film, respectively (color online).

generation of fluorescence from these radical molecules, which indicated efficient photothermal conversion and potential application in photothermal therapy field.

### 3.2 The stability and ground states of aromatic nitric acid radicals

These conjugated nitroxide radicals exhibited typical organic semiconductor properties and strong electro-chemical stability (Figure 3). The highest occupied molecular orbital (HOMO) and lowest unoccupied molecular orbital (LUMO)

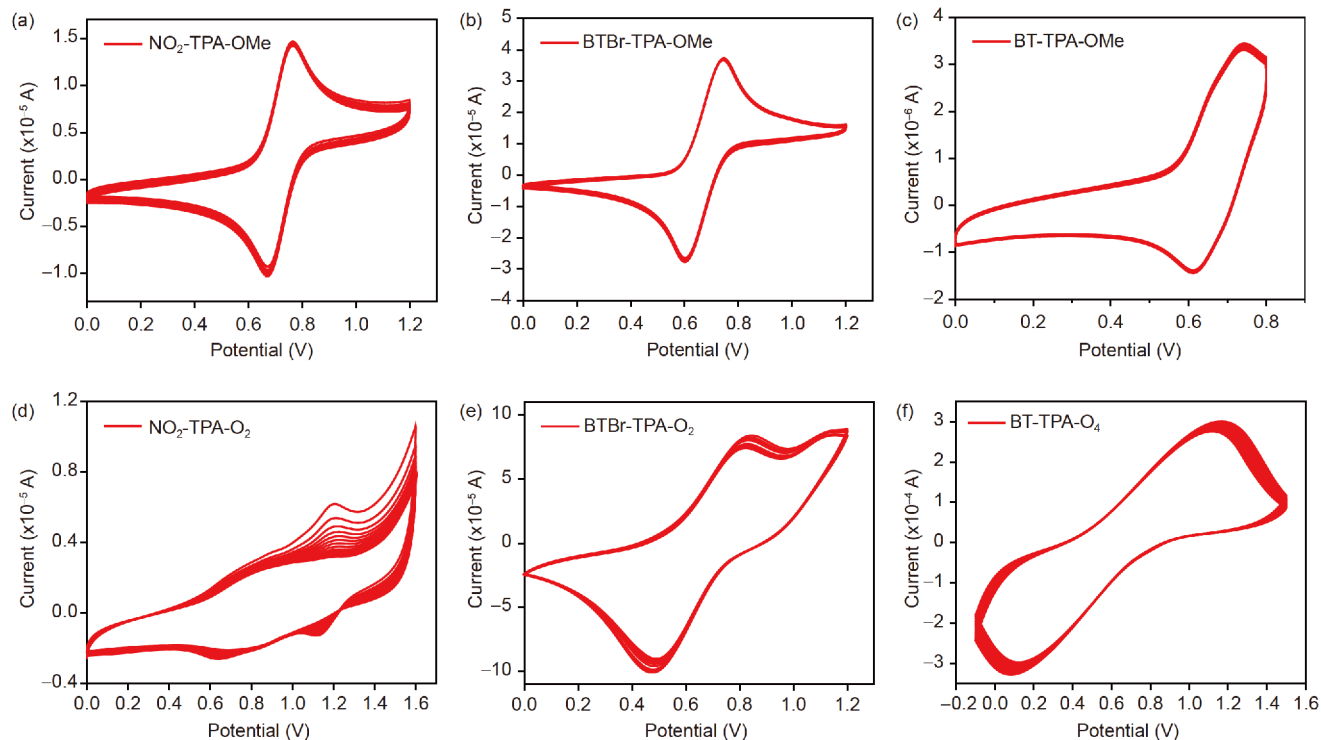


**Figure 3** Electrochemical stability results of (a)  $\text{NO}_2\text{-TPA-OMe}$ , (b)  $\text{BTBr-TPA-OMe}$  and (c)  $\text{BT-TPA-OMe}$  as well as demethylated counterparts (d)  $\text{NO}_2\text{-TPA-O}_2$ , (e)  $\text{BTBr-TPA-O}_2$  and (f)  $\text{BT-TPA-O}_4$ , respectively. All of CV curves were measured 15 cycles in dichloromethane solution containing 0.1 M  $n\text{Bu}_4\text{NPF}_6$  as a supporting electrolyte and the scan rate was 0.1 V/s. The methoxy substituted precursors were dissolved in dichloromethane at a concentration of 5 mg/mL and target radical compounds coated on carbon-glass electrode to form film during measurements. Potential values are reported with saturated calomel electrode as the reference electrode using the  $\text{Fc}^+/\text{Fc}$  couple (0.27 V) as an internal standard (color online).

energy levels were listed in Table S1 (Supporting Information online). The HOMO energy levels of demethylated counterparts  $\text{NO}_2\text{-TPA-O}_2$ ,  $\text{BTBr-TPA-O}_2$  and  $\text{BT-TPA-O}_4$  are recorded from CV measurements as  $-5.06$ ,  $-5.08$  and  $-5.02$  eV, respectively. The HOMO energy levels have been improved compared with the corresponding value  $-5.16$ ,  $-5.13$  and  $-5.10$  eV of methoxy substituted precursors, respectively. The symmetrical bisphenolamine radical  $\text{BT-TPA-O}_4$  serves as a conjugated extension of nitroxides such as TEMPO radical, equipped with analogous redox behavior and strongest stability in Figure 3(f) [29]. The redox behavior of  $\text{BT-TPA-O}_4$  showed the excellent reversibility of conjugated nitroxides structure. Besides, this conjugated nitroxide structure showed good thermal stability, exhibiting equivalent spin concentrate for  $\text{BT-TPA-O}_4$  exposed to air at room temperature after high temperature measurements in Figure 4. Furthermore, considering the contribution of the existence of rich resonance structures and the push-pull effect between the bisphenolamine donor and BT acceptor, the extended conjugation effects in aromatic nitroxides also response to the excellent electrochemical and thermal stability of  $\text{BT-TPA-O}_4$  [44]. This result provides us a ready route to obtain stable low band gap and stable radical semiconductors.

It is known that the ground state of these molecules are important issues to understand due to the different odd and

even number positions of free electrons in these molecules [37]. ESR measurements were applied to study the ground state of these stable radicals. It can be observed from Figures S7–S9 that there has been significant increase in the relative intensity of electron spin resonance after demethylation, due to the large amounts of radical generation with oxidation of phenolic hydroxyl in air. In addition, the  $g$  values of  $\text{NO}_2\text{-TPA-O}_2$ ,  $\text{BTBr-TPA-O}_2$  and  $\text{BT-TPA-O}_4$  are subtle different indicating diverse delocalization of radicals (Scheme 1(f)). This also explains the existence of shoulder side peak in the typical ESR spectrum (Figure S9) of  $\text{BT-TPA-O}_4$ . Besides, the ESR signal intensities from high to low are  $\text{BTBr-TPA-O}_2$ ,  $\text{NO}_2\text{-TPA-O}_2$  and  $\text{BT-TPA-O}_4$  under the same tested amount.

To further investigate the electronic structures and radical properties, we carried out variable temperature ESR (VT-ESR) measurement for  $\text{BT-TPA-O}_4$  under argon atmosphere at low temperature and high temperature zone, respectively. The ESR signal intensity increased with increasing temperature from room temperature (RT) to 500 K in Figure 5 (b). It is reasonable the enhanced ESR signal stems from the growing excited triplet state at the elevated temperature. Importantly, this result excludes the statement that the generation of free radicals originates from the doping of oxygen or other impurities. The singlet-triplet energy gap ( $\Delta E_{\text{S-T}}$ ) of  $\text{BT-TPA-O}_4$  was estimated by superconducting quantum in-

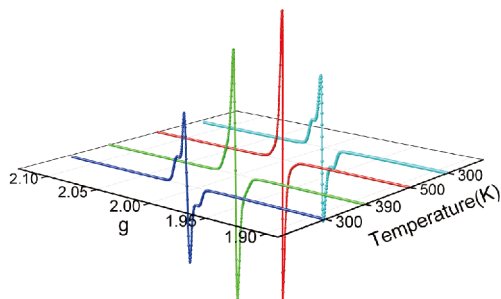


**Figure 4** ESR spectra of BT-TPA-O<sub>4</sub> in powder (28.5 mg, 0.0415 mmol, Attenuation=14 dB) measured at room temperature after experiencing high temperature measurements (color online).

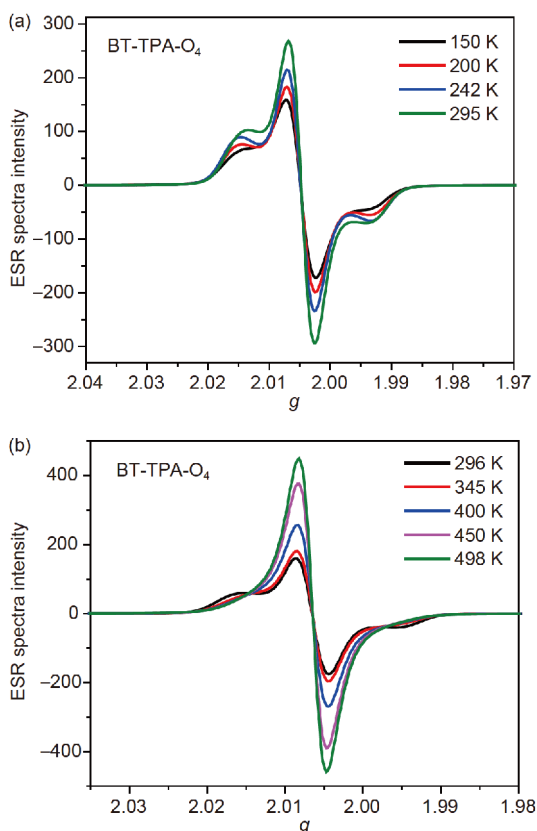


**Figure 5** (a) ESR spectra of BT-TPA-O<sub>4</sub> in powder (28.5 mg, 0.0415 mmol, Attenuation=14 dB) measured at 150, 200, 242 and 295 K, respectively; (b) ESR spectra of BT-TPA-O<sub>4</sub> in powder (28.5 mg, 0.0415 mmol, Attenuation=14 dB) measured at 296, 345, 400, 450 and 498 K, respectively. The paramagnetic tube was filled with argon during the measurement. The different dewars were used in low temperature and high temperature tests (color online).

terfering device (SQUID) measurements for a powder sample at the range of 2–400 K. Data from 2 to 250 K were fitted by modified Bleaney-Bowers equation and gave a  $\Delta E_{S-T} = -0.749$  kcal/mol (Figure 6), indicating that BT-TPA-O<sub>4</sub> had a singlet open-shell ground state. Besides, the spin-triplet of BTBr-TPA-O<sub>2</sub> was detected with the forbidden resonance resulting from  $\Delta MS = \pm 2$  (Figure 7), suggesting BTBr-TPA-

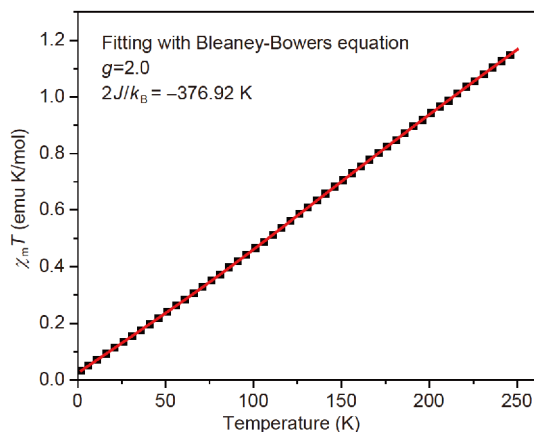


**Figure 6**  $\chi T$ - $T$  plot for the solid BT-TPA-O<sub>4</sub>. The measured data from 2 to 250 K were fitted by modified Bleaney-Bowers equation (color online).

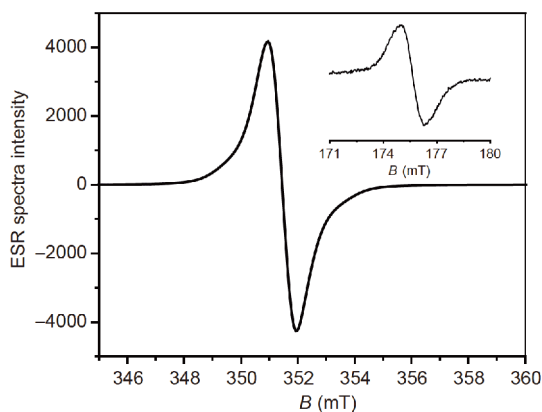


**Figure 7** ESR spectra of BTBr-TPA-O<sub>2</sub> (9.8 mg, 0.02 mmol, Attenuation=20 dB) in powder at room temperature. Inset: the forbidden  $\Delta MS = \pm 2$  resonance (Attenuation=4 dB) at room temperature (color online).

O<sub>2</sub> Curie-like behavior and an excited triplet state of BTBr-TPA-O<sub>2</sub> [12,13].

### 3.3 The proposed mechanism of AIAR

In previous work, there are reports on bis(triarylamine) dications isolated by using the weakly coordinating anions  $[Al(ORF)_4]^-$  as the counterions [45–47]. It is completely different to explain the origin of radical in term of phenylamine radicals. The singlet ground states of NO<sub>2</sub>-TPA-O<sub>2</sub> and BTBr-TPA-O<sub>2</sub> can be understood by our proposal on the formation and stabilization of diradicals in Scheme 1(d, e) considering the even (1-/16-) positions of two radicals in NO<sub>2</sub>-TPA-O<sub>2</sub> and BTBr-TPA-O<sub>2</sub>. The stability of NO<sub>2</sub>-TPA-O<sub>2</sub> and BTBr-TPA-O<sub>2</sub> comes from the highly efficient delocalization of diradicals in them. The inherent mechanism is different from the stability from the steric hindrance effect of phenoxy and TEMPO radicals [33]. Therefore, the introduction of strong electron-withdrawing groups and extended conjugation contribute to stabilize radicals in thermodynamic and achieve tunable ground states. Our re-

sults are different from the previous work [33], and our proposal is more reasonable to explain the singlet ground states as the two electrons can be localized on the 1-/16-positions of NO<sub>2</sub>-TPA-O<sub>2</sub> and BTBr-TPA-O<sub>2</sub> molecules (Scheme 1(c, d)).

For all methoxy and hydroxy substituted precursors, their ground-state geometries are optimized at B3LYP/6-31G\* level of theory. There is almost no significant change in the optimized structure with the substitution of hydroxyl to methoxy for NO<sub>2</sub>-TPA-OMe (Figures S10, S11), BTBr-TPA-OMe (Figures S13, S14) and BT-TPA-OMe (Figures S16, S17). The optimized result is consistent with similar UV-Vis absorption characteristics of methoxy and hydroxy substituted compounds. The geometry optimization of BT-TPA-O<sub>4</sub> (Figure 8) is investigated with UB3LYP/6-31G\* level of theory, suggesting that all phenoxy groups are quinoidal structures with remarkable reduced dihedral angle (C20-C19-N2-C13: 32.08°), contributing to strong absorption in NIR region because of better molecular planarity and electron delocalization. The situation is mirrored for NO<sub>2</sub>-TPA-O<sub>2</sub> (Figure S12) and BTBr-TPA-O<sub>2</sub> (Figure S15) that the C–N bonds and C–O bonds change from single bond to nitro-like closed-shell structure, contributing to expected thermal and electrochemical stability without steric hindrance protection of tertiary butyl. This result is similar to the previous report that triphenylamine phenoxy radical (Scheme 1(b)) possesses closed-shell electron structure and C–N bonds

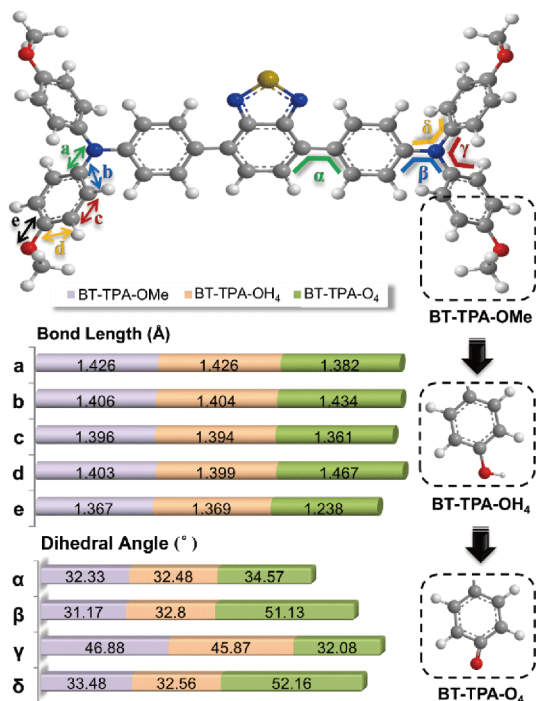


**Figure 8** The geometry optimizations of BT-TPA-OMe (B3LYP/6-31G\*), BT-TPA-OH<sub>4</sub> (B3LYP/6-31G\*) and BT-TPA-O<sub>4</sub> (UB3LYP/6-31G\*) were performed. Inset: the selected bond lengths and dihedral angles. Addition information can be found in [Supporting Information online](#) (Figures S16–S18) (color online).

have multiple-bond character [33]. However, it is hard to explain that phenolamine radicals in this work exhibit remarkable paramagnetic properties and singlet ground state in ESR and SQUID measurements according to the previous mechanism. It will be more reasonable that the AIAR mechanism is proposed to explain the stability and paramagnetism of these phenolamine radicals, compared with the previous work [33].

Phenolamine radicals could be generated due to the transformation from the nitro-like closed-shell structure to open-shell aromatic nitroxides, driven by the aromaticity and torsion angle of phenoxy groups. Besides, the aromatic nitric acid could be regarded as a class of conjugated nitroxide radicals, which will process two types of resonance structures including closed-shell nitro-like and open-shell diradical. To investigate the stability of different geometries, the single energy and spin density distribution of three kinds of neutral conjugated nitroxide radicals in the closed-shell, open-shell singlet and open-shell triplet states are performed with B3LYP/6-311++G\*\* level of theory (Figure 9). The calculated results (Table S2) show that the singlet ground states of NO<sub>2</sub>-TPA-O<sub>2</sub>, BTBr-TPA-O<sub>2</sub> and BT-TPA-O<sub>4</sub> are at a similar energy with the closed-shell structures, which boosts to stabilize the radical without steric hinderance protection. Besides, the triplet states with slightly higher energy explain the extremely strong ESR intensity at room temperature and are in accordance with the measurement results of ESR and SQUID. Therefore, the singlet ground state diradicals indicate that diradicals will be induced with the formation of the quinoid structure of backbone in the aggregation state, i.e. aggregation-induced radical (AIR). The formation of the quinoid-diradical structure is similar to our previous work on the low bandgap semiconductors [44].

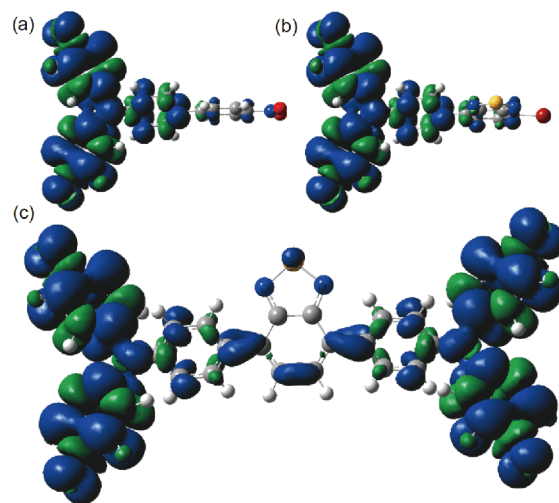


**Figure 9** The spin density distribution of (a) NO<sub>2</sub>-TPA-O<sub>2</sub>, (b) BTBr-TPA-O<sub>2</sub> and (c) BT-TPA-O<sub>4</sub> in the open-shell triplet states, respectively. Blue and green surfaces represent α and β spin density, respectively (color online).

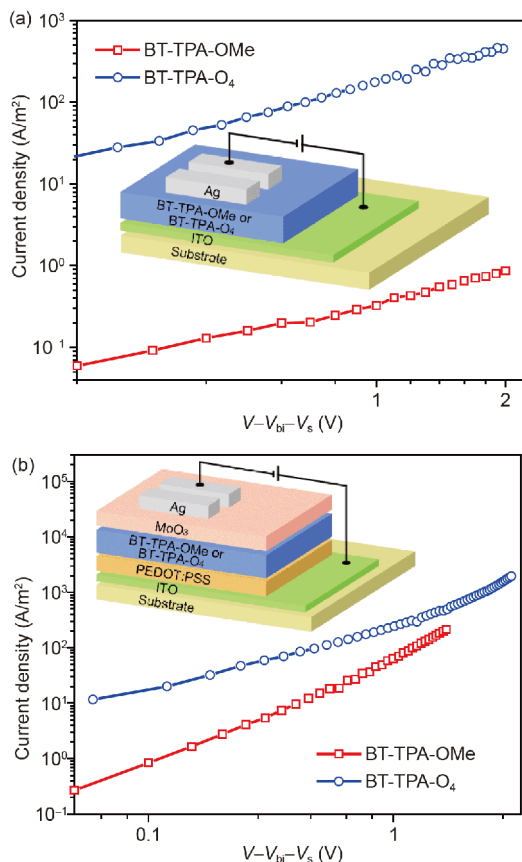


**Figure 10** Experimental  $J$ - $V$  characteristics of different devices with space charge limited current fitting for BT-TPA-OMe and BT-TPA- $O_4$ , respectively. (a)  $J$ - $V$  characteristics of ITO/BT-TPA-OMe or BT-TPA- $O_4$ /Ag devices; (b)  $J$ - $V$  characteristics of ITO/PEDOT:PSS/BT-TPA-OMe or BT-TPA- $O_4$ /Mo $O_3$ /Ag hole-only devices (color online).

The excited triplet state with the configuration of multiple aromatic phenyl group will be observed by ESR via thermal excitation, as shown in [Scheme 1](#). The existence of rich resonance structures supports their unexpected strong thermal and electrochemical stability, interesting paramagnetism and tunable ground states. This strategy can also be applied to the aromatization of other inorganic acids including  $H_2CO_3$ ,  $H_2SO_4$  and  $H_3PO_4$  to obtain AIARs and prepare potential diradicals with triplet ground states.

### 3.4 The enhanced hole mobility of aromatic nitric acid radical

The hole mobilities of BT-TPA-OMe and BT-TPA- $O_4$  were evaluated with the hole-only devices fabricated with different device structure as the inset of [Figure 10](#). The hole mobility of pristine BT-TPA- $O_4$  film was obviously enhanced compared to BT-TPA-OMe ([Figure 10\(a\)](#)). The hole mobility of BT-TPA- $O_4$  can be significantly enhanced by three orders of magnitude comparing with BT-TPA-OMe in this device structure due to the suitable HOMO level of  $-4.81$  eV, which matches well with ITO. In the device of [Figure 10\(b\)](#), the

hole mobilities of BT-TPA-OMe and BT-TPA- $O_4$  were calculated to be  $7.1 \times 10^{-5}$  and  $2.3 \times 10^{-4}$   $cm^2/(V s)$ , respectively, by fitting the data using the space charge limited current (SCLC) model with the classical device structure [48]. The enhancement of the hole mobility of BT-TPA- $O_4$  is ascribed to the quinoid resonance structure, good electron delocalization and lowered band gap, contributing to highly efficient hole injection and enhanced hole mobility. Besides, considering inherent high spin concentration, AIARs will probably exhibit a highly enhanced conductivity in its non-doped state. This provides us a new concept for the design of organic semiconductors with high charge mobility. Furthermore, considering the high spin density of these stable radicals, the work to introduce highly planar and conjugated polyradicals is under progress in our lab. These materials might show different electron transport behaviors from traditional organic semiconductors and half-metallic or metallic characteristics as exact synthetic metals.

## 4 Conclusions

In summary, we discovered and reported three new phenolamine radicals that showed unexpected stability and low band gap. The good thermal stability at elevated temperature as well as electrochemical stability comes from their distinctive aromatic nitro-like resonance structure. The introduction of strong electron-withdrawing groups, extended conjugation and enhanced electron delocalization contribute to the stability of radicals and tunable ground states. Furthermore, the conjugated nitroxide radicals could be obtained by a simple synthetic route and exhibited absorption in the NIR region as well as obvious enhancement of hole mobility. Meanwhile, it is worthy to mention that we, for the first time, proposed a novel viewpoint to understand the formation of radicals motivated from aromatization of  $HNO_3$ , which are different from previous radical materials. This strategy can also be applied to the aromatization of other inorganic acids including  $H_2CO_3$ ,  $H_2SO_4$  and  $H_3PO_4$ , thus developing stable high-spin AIAR materials with planar and highly conjugated structure for application in electronic, spintronic and magnetic devices.

**Acknowledgements** This work was supported by the Pearl River S&T Nova Program of Guangzhou (201710010194), the National Natural Science Foundation of China (61574061, 21520102006, 21634004, 51521002, 91633301), and the Foundation of Guangzhou Science and Technology Project (201707020019).

**Conflict of interest** The authors declare that they have no conflict of interest.

**Supporting information** The supporting information is available online at <http://chem.scichina.com> and <http://link.springer.com/journal/11426>. The supporting materials are published as submitted, without typesetting or editing. The responsibility for scientific accuracy and content remains entirely with the authors.

- 1 Joo Y, Agarkar V, Sung SH, Savoie BM, Boudouris BW. *Science*, 2018, 359: 1391–1395
- 2 Kamada K, Ohta K, Kubo T, Shimizu A, Morita Y, Nakasuji K, Kishi R, Ohta S, Furukawa S, Takahashi H, Nakano M. *Angew Chem Int Ed*, 2007, 46: 3544–3546
- 3 Fujita W, Awaga K. *Science*, 1999, 286: 261–262
- 4 Ai X, Chen Y, Feng Y, Li F. *Angew Chem Int Ed*, 2018, 57: 2869–2873
- 5 Son YW, Cohen ML, Louie SG. *Nature*, 2006, 444: 347–349
- 6 Yuan D, Guo Y, Zeng Y, Fan Q, Wang J, Yi Y, Zhu X. *Angew Chem Int Ed*, 2019, 58: 4958–4962
- 7 Morita Y, Nishida S, Murata T, Moriguchi M, Ueda A, Satoh M, Arifuku K, Sato K, Takui T. *Nat Mater*, 2011, 10: 947–951
- 8 Abe M, Ye J, Mishima M. *Chem Soc Rev*, 2012, 41: 3808–3820
- 9 Thiele J, Balhorn H. *Ber Dtsch Chem Ges*, 1904, 37: 1463–1470
- 10 Tschitschibabin AE. *Ber Dtsch Chem Ges*, 1907, 40: 1810–1819
- 11 Sun Z, Ye Q, Chi C, Wu J. *Chem Soc Rev*, 2012, 41: 7857–7889
- 12 Ito A, Urabe M, Tanaka K. *Angew Chem Int Ed*, 2003, 42: 921–924
- 13 Isogai A, Saito T, Fukuzumi H. *Nanoscale*, 2011, 3: 71–85
- 14 Abe M. *Chem Rev*, 2013, 113: 7011–7088
- 15 Xue Q, Liu M, Li Z, Yan L, Hu Z, Zhou J, Li W, Jiang XF, Xu B, Huang F, Li Y, Yip HL, Cao Y. *Adv Funct Mater*, 2018, 28: 1707444
- 16 Hu X, Chen H, Zhao L, Miao M, Han J, Wang J, Guo J, Hu Y, Zheng Y. *Chem Commun*, 2019, 55: 7812–7815
- 17 Nakagaki T, Sakai T, Mizuta T, Fujiwara Y, Abe M. *Chem Eur J*, 2013, 19: 10395–10404
- 18 Chase DT, Fix AG, Kang SJ, Rose BD, Weber CD, Zhong Y, Zakharov LN, Lonergan MC, Nuckolls C, Haley MM. *J Am Chem Soc*, 2012, 134: 10349–10352
- 19 Shimizu A, Kubo T, Uruichi M, Yakushi K, Nakano M, Shiomi D, Sato K, Takui T, Hirao Y, Matsumoto K, Kurata H, Morita Y, Nakasuji K. *J Am Chem Soc*, 2010, 132: 14421–14428
- 20 Kubo T, Sakamoto M, Akabane M, Fujiwara Y, Yamamoto K, Akita M, Inoue K, Takui T, Nakasuji K. *Angew Chem Int Ed*, 2004, 43: 6474–6479
- 21 Li Y, Heng WK, Lee BS, Aratani N, Zafra JL, Bao N, Lee R, Sung YM, Sun Z, Huang KW, Webster RD, López Navarrete JT, Kim D, Osuka A, Casado J, Ding J, Wu J. *J Am Chem Soc*, 2012, 134: 14913–14922
- 22 Hoover JM, Ryland BL, Stahl SS. *J Am Chem Soc*, 2013, 135: 2357–2367
- 23 Habibi Y, Lucia LA, Rojas OJ. *Chem Rev*, 2010, 110: 3479–3500
- 24 Benoit D, Chaplinski V, Braslau R, Hawker CJ. *J Am Chem Soc*, 1999, 121: 3904–3920
- 25 Quinkert G, Wiersdorff WW, Finke M, Opitz K. *Tetrahedron Lett*, 1966, 7: 2193–2200
- 26 Kolc J, Michl J. *J Am Chem Soc*, 1973, 95: 7391–7401
- 27 McMasters DR, Wirz J. *J Am Chem Soc*, 2001, 123: 238–246
- 28 McMasters DR, Wirz J, Snyder GJ. *J Am Chem Soc*, 1997, 119: 8568–8569
- 29 Amorati R, Pedulli GF, Pratt DA, Valgimigli L. *Chem Commun*, 2010, 46: 5139–5141
- 30 Altwicker ER. *Chem Rev*, 1967, 67: 475–531
- 31 Coppinger GM. *J Am Chem Soc*, 1957, 79: 501–502
- 32 Yang NC, Castro AJ. *J Am Chem Soc*, 1960, 82: 6208
- 33 Sakamaki D, Yano S, Kobashi T, Seki S, Kurahashi T, Matsubara S, Ito A, Tanaka K. *Angew Chem Int Ed*, 2015, 127: 8385–8388
- 34 Shimizu D, Fujimoto K, Osuka A. *Angew Chem Int Ed*, 2018, 57: 9434–9438
- 35 Waked AE, Ostadsharif Memar R, Stephan DW. *Angew Chem Int Ed*, 2018, 57: 11934–11938
- 36 Wang J, Kim G, Sandoval-Salinas ME, Phan H, Gopalakrishna TY, Lu X, Casanova D, Kim D, Wu J. *Chem Sci*, 2018, 9: 3395–3400
- 37 Li Y, Huang KW, Sun Z, Webster RD, Zeng Z, Zeng W, Chi C, Furukawa K, Wu J. *Chem Sci*, 2014, 5: 1908–1914
- 38 Yanai T, Tew DP, Handy NC. *Chem Phys Lett*, 2004, 393: 51–57
- 39 Lee C, Yang W, Parr RG. *Phys Rev B*, 1988, 37: 785–789
- 40 Mihailitchi VD, van Duren JKJ, Blom PWM, Hummelen JC, Janssen RAJ, Kroon JM, Rispens MT, Verhees WJH, Wienk MM. *Adv Funct Mater*, 2003, 13: 43–46
- 41 Zhang Y, de Boer B, Blom PWM. *Adv Funct Mater*, 2009, 19: 1901–1905
- 42 Crystallographic data for TPA-OH<sub>2</sub>: C<sub>18</sub>H<sub>15</sub>NO<sub>2</sub>,  $M_w=277.31$ ; monoclinic; space group  $I2/a$ ;  $a=17.7458(4)$  Å,  $b=7.60935(14)$  Å,  $c=21.3425(5)$  Å,  $\alpha=90^\circ$ ,  $\beta=100.335(2)^\circ$ ,  $\gamma=90^\circ$ ;  $V=2835.21(10)$  Å<sup>3</sup>;  $Z=8$ ;  $\rho_{\text{calc}}=1.299$  g/cm<sup>3</sup>;  $R_1=0.0377$  ( $I>2\sigma(I)$ ),  $wR_2=0.1037$  (all data). CCDC No. 1908983. X-ray-quality crystal was obtained by slow evaporation of the solution in dichloromethane/petroleum ether.
- 43 Wang Y, Qiu S, Xie S, Zhou L, Hong Y, Chang J, Wu J, Zeng Z. *J Am Chem Soc*, 2019, 141: 2169–2176
- 44 Li Y, Li L, Wu Y, Li Y. *J Phys Chem C*, 2017, 121: 8579–8588
- 45 Su Y, Wang X, Wang L, Zhang Z, Wang X, Song Y, Power PP. *Chem Sci*, 2016, 7: 6514–6518
- 46 Pan X, Chen X, Li T, Li Y, Wang X. *J Am Chem Soc*, 2013, 135: 3414–3417
- 47 Tan G, Wang X. *Acc Chem Res*, 2017, 50: 1997–2006
- 48 Xue Y, Wu Y, Li Y. *J Power Sources*, 2017, 344: 160–169